Journal of Power Sources 196 (2011) 1992–2004

Contents lists available at ScienceDirect

Journal of Power Sources

journal homepage: www.elsevier.com/locate/jpowsour

Predicting current density distribution of proton exchange membrane fuel cells with different flow field designs

Yong-Song Chen [a,*], Huei Peng [b]

[a] Chung-Shan Institute of Science & Technology, Materials & Electro-Optics Research Division, P.O. Box No. 90008-8-3 Longtan, Taoyuan 325, Taiwan, ROC
[b] Department of Mechanical Engineering, University of Michigan, Ann Arbor, MI, United States

ARTICLE INFO

Article history:
Received 7 July 2010
Received in revised form
27 September 2010
Accepted 29 September 2010
Available online 7 October 2010

Keywords:
Proton exchange membrane fuel cell
Flow field
Current density
Water accumulation
Modeling

ABSTRACT

In a proton exchange membrane fuel cell (PEMFC), flow field design is an important factor that influences the distributions of current density and water accumulation. The segmented model developed in prior study is used to investigate the effect of flow field patterns on current density distribution. This model predicts the distributed characteristics of water content in the membrane, relative humidity in the flow channels, and water accumulation in the gas diffusion layers (GDLs).

Three single cells with different flow field patterns are designed and fabricated. These three flow field designs are simulated using the segmented model and the predicted results are compared and validated by experimental data. This segmented model can be used to predict the effect of flow field patterns on water and current distributions before they are machined.

1. Introduction

The performance of a PEMFC is influenced by operating conditions such as current and temperature, and cell designs [1,2]. Among the fuel cell stack operating conditions, temperature, flow rates, pressure, and relative humidity (RH) of reactants are key factors that affect membrane hydration level, and thus the electrical conductivity of the membrane. As to the cell designs, flow field patterns on the bipolar plates play an important role in distributing reactants evenly throughout the cell, and avoid flooding by removing generated liquid water.

A PEMFC stack consists of multiple cells connected by bipolar plates. They account for the majority of stack volume and weight. The bipolar plates play multiple roles such as current distribution and collection, transporting and distributing reactants, and removing generated liquid water. The power density of a PEMFC can be significantly influenced by the flow channel patterns on the bipolar plates. An appropriate flow field design can increase the power density and improve water and heat managements. In some designs, cooling channels are integrated on the bipolar plates [3,4]. Thus, the flow field pattern on the bipolar plates is an important factor in the design of a PEMFC stack.

Common flow field patterns include parallel, serpentine, interdigitated as well as their combinations. Um et al. [5] used computational fluid dynamics (CFD) method to develop a three-dimensional model to study the performance of an interdigitated flow field design. Their results show improved performance of fuel cell due to forced convection of gases through the gas GDL. Wang et al. [6] and Pasaogullari and Wang [7] developed a two-phase flow model for the cathode GDL, which successfully described water vapor distribution and liquid water accumulation in the GDL and in the flow channel. Due to heavy computation load, CFD models usually have difficulties simulating a fuel cell with a complicated flow field pattern. Thus, the published CFD models typically were demonstrated using a fuel cell with simple flow field such as a straight flow channel.

Many studies have compared the performance of fuel cells with different flow field designs. Aricò et al. [8] conducted an experiment to compare the influence of the flow field design on the performance of direct methanol fuel cells (DMFCs). Dohle et al. [9] and Bewer et al. [10,11] also investigated the influence of flow field design on the performance of PEMFCs. They concluded that flow field patterns can significantly affect the distribution of gas flow and current density of a PEMFC.

Kumar and Reddy [12] developed a three-dimensional single phase isothermal model to describe the steady-state and transient response of four PEMFCs with different flow field designs, including serpentine, parallel, multi-parallel, and interdigitated types. Their modeling results showed that transient responses of

* Corresponding author. Tel.: +886 2 26712711x313860; fax: +886 2 26721134.
E-mail address: songchen@umich.edu (Y.-S. Chen).

0378-7753/$ – see front matter © 2010 Elsevier B.V. All rights reserved.
doi:10.1016/j.jpowsour.2010.09.094

Nomenclature

a	water vapor activity
F	Faraday's constant (96,485 C equivalent^{-1})
I	current (A)
N	molar flow rate (mol s^{-1})
P	pressure (Pa)
V	voltage (V)
Greek	
λ	water content
Subscripts	
an	anode
avg	average
ca	cathode
cell	cell
H_2	hydrogen
in	inlet
N_2	nitrogen
out	outlet
O_2	oxygen
pem	proton exchange membrane
seg	segment
w	liquid water

serpentine and parallel designs were faster but performances were lower than the other two designs. However, Kumar's study did not consider water accumulation in the GDLs. Due to heavy computational method, their model was not able to simulate PEMFCs with different anode and cathode flow field designs.

Lumped models which assume uniform reactions within the whole area of the fuel cells do not consider the spatial distribution of reactants. Golbert and Lewin [13] developed a dynamic fuel cell model, which accounts for spatial dependencies of voltage, current, reactant flows, and temperatures in the flow channel. However, their model can only describe the transient behavior within a single straight flow channel. In practice, the fuel cell performance and water distribution depend on flow field design, and the water generation and accumulation inside the fuel cells distribute unevenly along the flow channels. A model that can describe the distributed properties of a single cell, especially with complex flow pattern, is needed.

In order to solve this problem, in our previous work [14] we developed a segmented model to predict distributions of liquid water accumulation, current density, water content in the membrane, and relative humidity in the flow channels. In this study, we use the segmented model to study four single cells with different flow field patterns. The performance and distributed properties of these single cells under various working conditions are simulated and discussed.

2. Modeling procedure

In this work, we design three single cells with different cathode flow field patterns, as shown in Fig. 1. These three designs represent popular straight channel, serpentine, and perpendicular/counter-flow flow field arrangements. Three models corresponding to these three patterns are also developed to study their influence on cell performance and water accumulation. The model calibration is done based on experimental data of the single cell No. 1. Then we keep the calibrated parameters and reconnect the segments within the models to simulate the flow field patterns of cells No. 2 and No. 3, respectively. The experimental results of cells No. 2 and No. 3 are used to validate modeling results. Based on the modeling results of these three patterns, this model approach was found to produce qualitatively accurate predictions. Subsequently, we designed a fourth flow pattern. The modeling results of these four cells are then analyzed and discussed. This design procedure is depicted in Fig. 2.

2.1. Summary of the segmented model

In this paper, we use the segmented model developed in our previous paper [14] to investigate the influence of flow field patterns on cell performance. The details of the model have been published; therefore, only the concept is summarized below.

To capture the distributed behavior inside a PEMFC, the active area is divided into fifteen segments and each segment is viewed as a small lumped model. These segments are connected together according to the flow field directions of the anode and cathode, as shown in Fig. 3. Each segment consists of six interacting sub-models: cathode flow channel, anode flow channel, cathode GDL, anode GDL, membrane hydration, and segment voltage. The model is implemented in MATLAB/SIMULINK. The block diagrams of these six sub-models of a segment are shown in Fig. 4. Given the inflow properties and (initial guess of) a segment current, each segment model calculates its segment voltage. Since the current density is actually not uniform throughout the active area, the calculated segment voltages may not be the same. Thus, the cell voltage is determined iteratively by the process shown in Fig. 5. This algorithm is explained briefly below.

At the beginning of an iteration, we guess an inlet gas pressure P_{in} for a certain load current I_{cell}. Under desired stoichiometry values and relative humidity levels, the inflow anode and cathode flow properties for the cell are determined. The initial guess for each segment current $I_{seg,i}$, is set to be one fifteenth of the cell current, I_{cell}. The segment voltage $V_{seg,i}$ is determined by the segment model. Because of different locations, each segment may not have the same inflow gas properties such as reactant pressure, relative humidity, and reactant concentration, resulting in different segment voltages—which in theory should be identical.

If the difference between the maximum and minimum segment voltages is not within an acceptable range, the segment currents need to be corrected. Based on the typical polarization curve of a fuel cell, the segment with higher voltage should have higher current, and the one with lower voltage should lower its current. To increase iteration speed, the change in segment current is set to be proportional to the voltage difference while keeping the cell current constant.

$$\Delta I_i = k[\max(V_{seg,i}) - \min(V_{seg,i})] \quad (1)$$

$$I_{seg,i}|^{n+1} = I_{seg,i}|^{n} + \frac{\Delta I_i}{\text{number of segments with } V_{seg,i} > V_{avg}} \quad \text{when } V_{seg,i} > V_{avg} \quad (2)$$

$$I_{seg,j}|^{n+1} = I_{seg,j}|^{n} - \frac{\Delta I_i}{\text{number of segments with } V_{seg,j} < V_{avg}} \quad \text{when } V_{seg,j} < V_{avg} \quad (3)$$

The superscript n in these equations indicates the n-th step in time. In addition, the inlet pressures of the anode and cathode are also adjusted to keep the outlet pressure the same as the ambient pressure. At the end of the iteration procedure, averaged values in each segment are calculated and assumed to represent the variable values at the center of each segment. These values are then used to

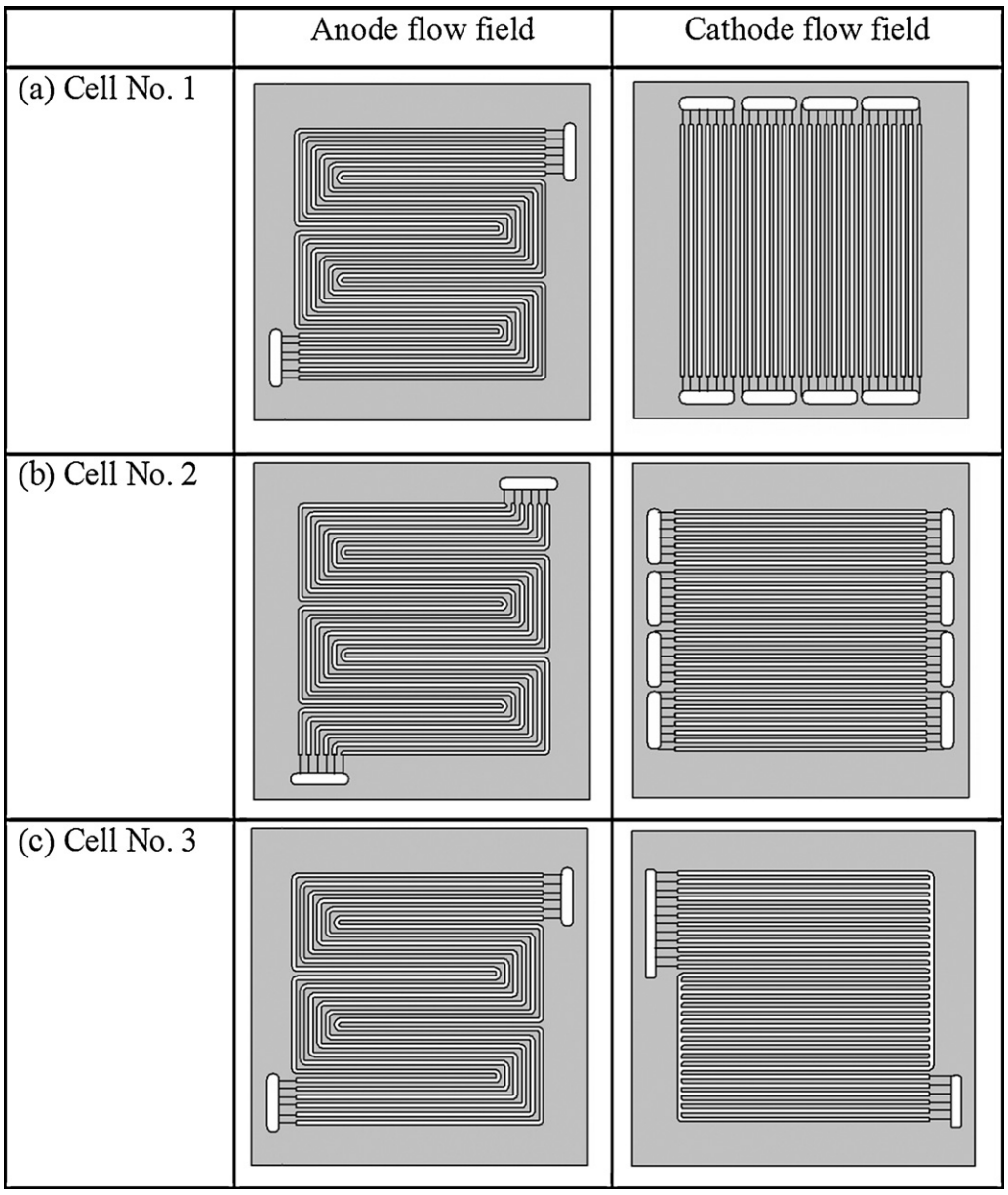

Fig. 1. Flow field designs in this study (Left: anode; Right: cathode.). (a) Cell No. 1; (b) cell No. 2; (c) cell No. 3.

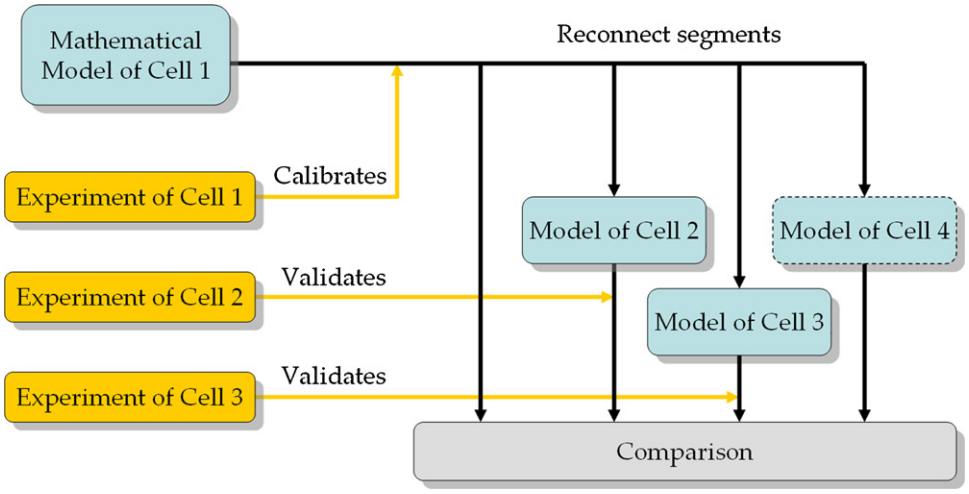

Fig. 2. Flow diagram showing modeling procedure.

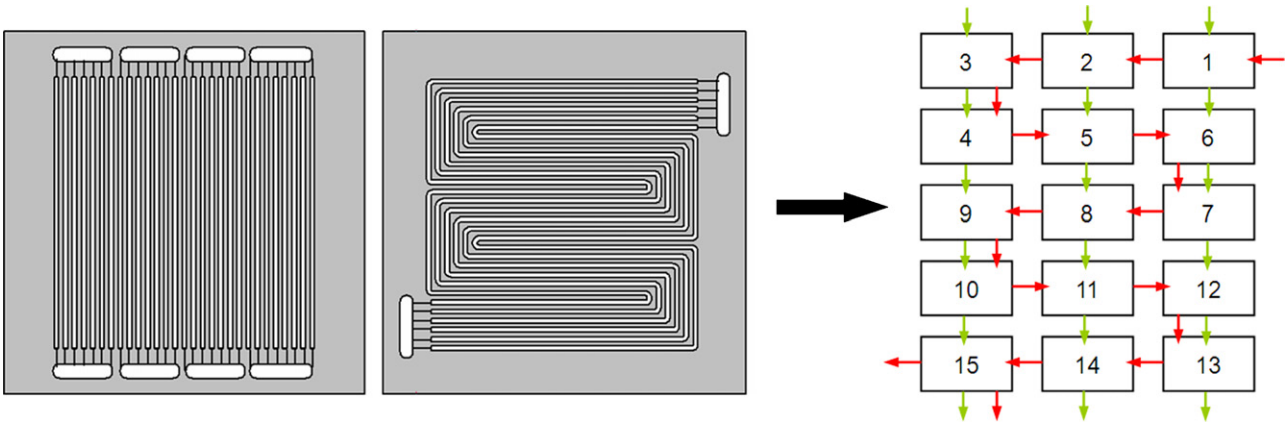

Fig. 3. Schematic of a single cell modeled as fifteen segments.

calculate the distributed values of the whole active area of the fuel cell through interpolation and extrapolation.

2.2. Modeling of counter-flow and co-flow designs

In the flow field patterns of cells No. 2 and No. 3, counter-flow exists in part of the active area, as shown in Fig. 6. Fig. 7 shows segments numbered successively according to the anode flow direction. If we follow the iteration procedure shown in Fig. 5, it will be a challenge in solving the counter-flow segments. In this study, segment current and all the properties of the anode and cathode reactants are required for individual segment to obtain the segment voltage. In the model of cell No. 2, if we solve each segment successively according to the anode flow direction, then there is no problem to get $N_{an,H_2,in}$ and $N_{an,w,in}$ for segments 1, 2, and 3. However, when we start to solve segment 4, we do not have the values of $N_{ca,O_2,in}$, $N_{ca,N_2,in}$, and $N_{ca,w,in}$ since they are outputs of segment 5, which has not been solved yet.

A few researchers have modeled the counter-flow configuration of PEMFCs [15–18]. Ge and Yi [15] developed a two dimensional model to investigate the co-flow and counter-flow modes at different operating conditions. When they dealt with the counter-flow mode, they guessed a water flow rate at the cathode inlet and the calculated water flow rate at the cathode outlet was compared with the actual value. If these two values do not match, they guess a new value and iterate through the process until convergence. Birgersson and Vynnycky [16] developed an isothermal three-dimensional model to compare the performance of four different flow field pat-

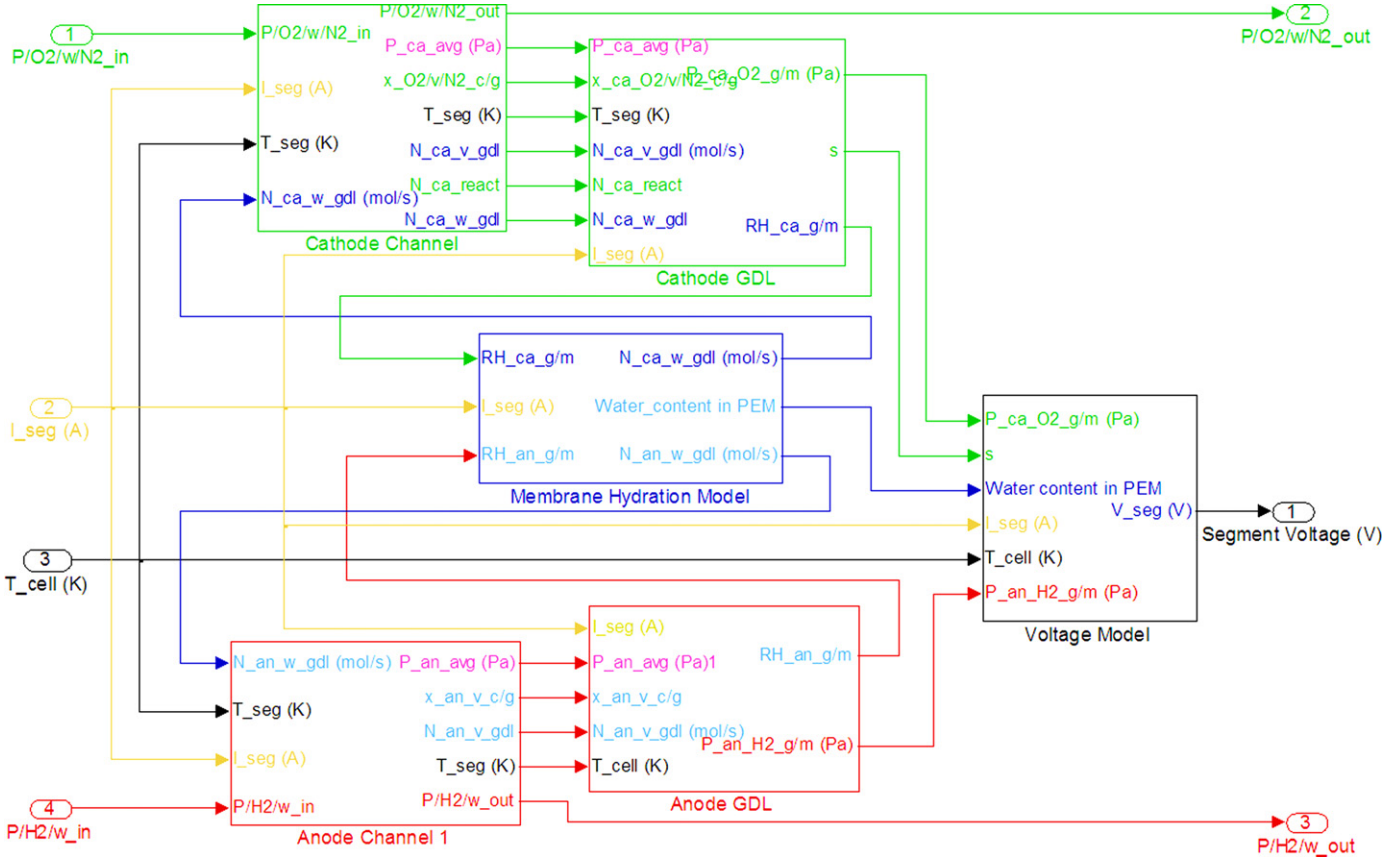

Fig. 4. The connection of the six sub-models of a segment in the SIMULINK environment.

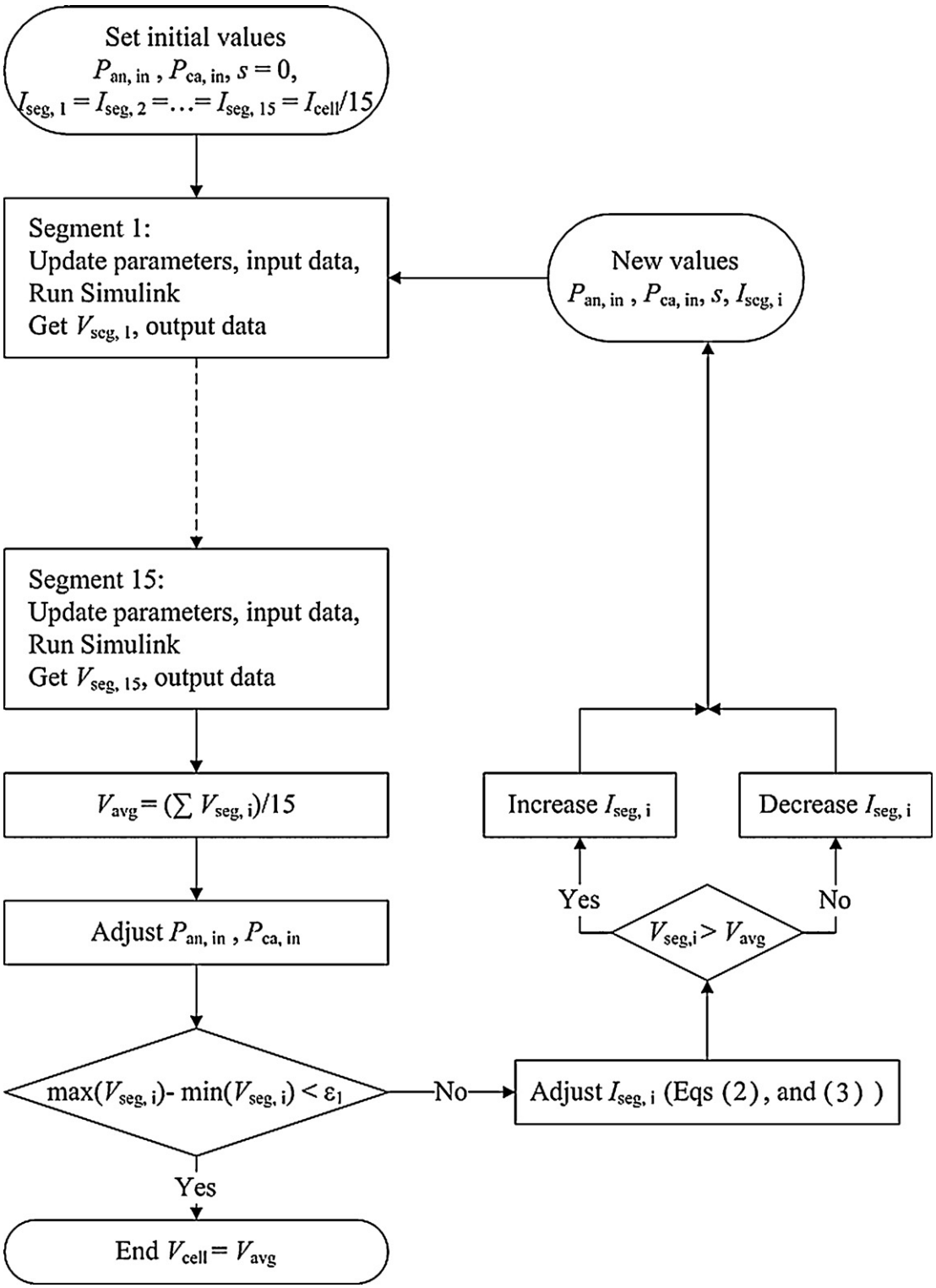

Fig. 5. Flow diagram of the iterative procedure to calculate cell voltage.

terns: co-flow, counter-flow, interdigitated, and foam. The details of solving counter-flow mode were not given in their study. However, their model took one to twelve hours to solve the counter-flow model problem. Their results suggested that under the same operating conditions, interdigitated and foam flow fields showed higher performance than co-flow and counter-flow did, but there was no significant performance difference between the co-flow and counter-flow. Hwang et al. [17] developed a non-isothermal model to investigate an interdigitated flow field pattern. They studied the conditions where the cathode reactants flowed into the GDL with the same (co-flow) and opposite (counter-flow) directions to the anode reactants. They used commercial software to solve their model and the details were not provided in their paper. Their model also took hours to solve for each operating condition.

Berger et al. [18] developed a simplified model to study the distributions of current density and relative humidity along a straight

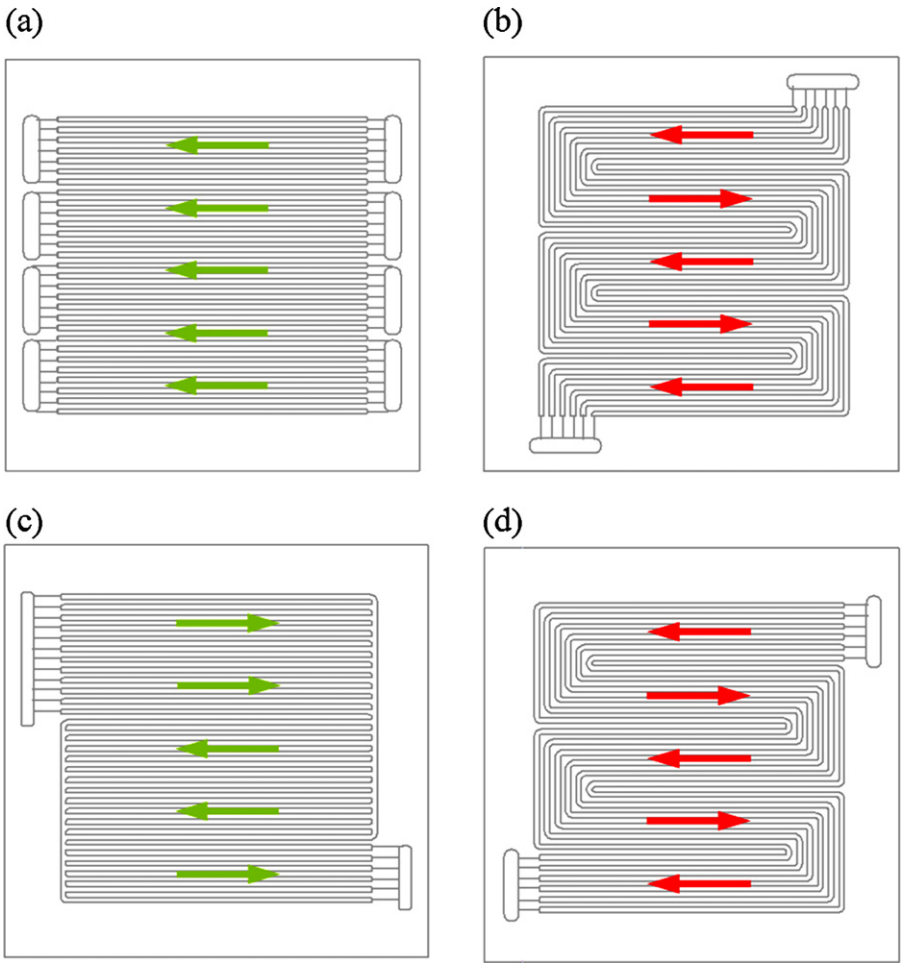

Fig. 6. Schematic representation of counter-flow and co-flow modes in cells No. 2 and No. 3. (a) Cathode of cell No. 2; (b) anode of cell No. 2; (c) cathode of cell No. 3; (b) anode of cell No. 3.

channel. They discussed the influences of co-flow and counter-flow modes on the distributions of current density and relative humidity. In their model they discretized the flow channel into 1048 points. When they solved the counter-flow mode, all the initial values of the anode and cathode fluxes at these points were set as the inlet values. The cathode fluxes were then updated by using the anode fluxes from the previous iteration. The anode fluxes were then updated by using local current and water transfer calculated from previously computed cathode channel values. The updating process is continued until the anode and the cathode flux values converge. The details can be found in Ref. [18]. This is a useful method for solving the counter-flow problem in a straight channel design. In our study, there are not only counter-flow modes but also co-flow modes in our designs of cells No. 2 and No. 3; moreover, the flow field patterns are not simply straight channels. Therefore, we used a modified version of Berger's updating procedure to solve the problem in our models.

As mentioned at the beginning of this section, $N_{ca,O_2,in}$, $N_{ca,N_2,in}$, and $N_{ca,w,in}$ for segment 4 are unknown when we start to solve segment 4 in cell No. 2 during each iteration. However, we can

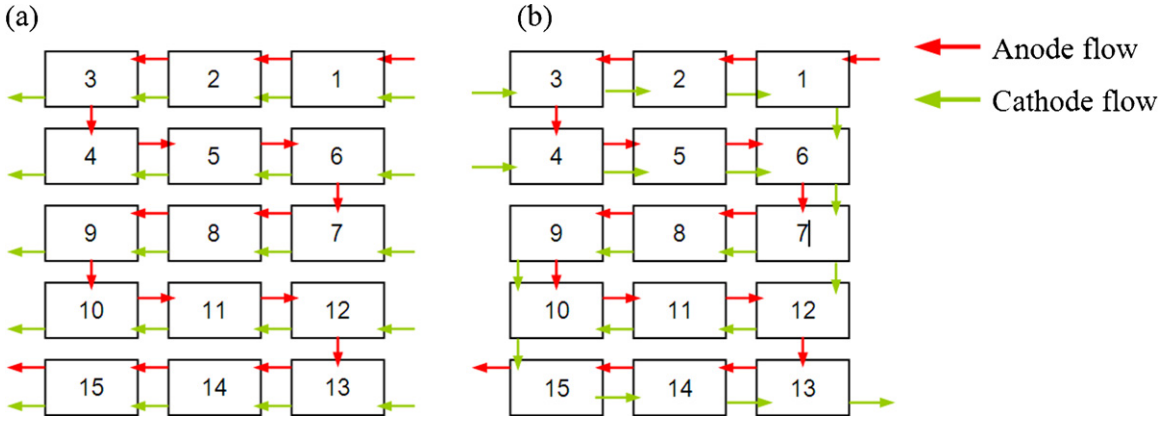

Fig. 7. Segment connection of cell No. 2 (a) and No. 3 (b).

calculate $N_{ca,O_2,in}$ and $N_{ca,N_2,in}$ before segment 5 and segment 6 are solved. Flow rates of reacted oxygen in segments 5 and 6 can be determined by the assigned segment currents at the beginning of each iteration.

$$N_{ca,O_2,in}\big|_{seg,4} = N_{ca,O_2,in}\big|_{seg,6} - \frac{I_{seg,5}}{4F} - \frac{I_{seg,6}}{4F} \quad (4)$$

Besides, nitrogen does not react, so nitrogen flow rate in segment 4 is equal to that at the inlet of segment 6.

$$N_{ca,N_2,in}\big|_{seg,4} = N_{ca,N_2,in}\big|_{seg,6} \quad (5)$$

Accordingly, the only unknown is $N_{ca,w,in}$ when we start to solve segment 4. In the flow field design of cell No. 2, same situation happens to segments 5, 10, and 11.

Similar to Berger's iteration procedure, in the beginning of our solution process, the $N_{ca,w,in}$ values of segments 4, 5, 10, and 11 are initially set as the inlet values of segments 6 or 12 based on the flow field pattern. Then $N_{ca,w,in}$ values of the above four segments are updated by using the output values of their preceding segments, i.e., segments 5, 6, 11, 12, respectively.

$$N_{ca,w,in}\big|_{seg,4}^{n+1} = N_{ca,w,out}\big|_{seg,5}^{n} \quad (6)$$

The superscript n in these equations indicates the n-th step in time. The updating procedure continues until solutions converge. The same solution procedure is applied to cell No. 3 for those segments with counter-flow mode.

The modeling results will be discussed in the next section. After this model is calibrated and validated by experimental data, it can be applied to other cells with different flow field designs.

3. Modeling results and discussions

3.1. Modeling results of cells No. 1, 2, and 3

Fig. 8 shows performance curves of cells No. 1, 2, and 3. All three cells operated at low cathode inlet RH of 50% show lower cell performance than at inlet RH of 100%. In addition, cell No. 1 shows lower performance than cells No. 2 and 3 when the cathode inlet RH is 50%. This is because of the low water content in the cathode gas flow, and in the design of cell No. 1, more water seems to be taken from the membrane, resulting in low membrane hydration and low conductivity, as shown in Fig. 8(b) and (c). The experimental results suggest that cathode inlet RH has more significant influence on cell performance in cell No. 1. A possible reason is because the counter-flow mode exists in both cells No. 2 and 3 which helps to improve membrane hydration and conductivity.

For the model developed to describe cell No. 1, the parameters were calibrated based on the experimental data. Fig. 8(a) shows that simulation results agree well with the experimental results after the model calibration. In Fig. 8(b) and (c), the slight deviation between modeling results and experimental results for cells No. 2 and No. 3 could indicate that the model calibrated well for one flow field design does not fully capture the cell with different cathode flow field designs, even after we reconnect the 15 segments properly. Another possible reason of this slight mismatch is that the MEAs used for the three single cells are not identical. For example, the difference of Pt catalyst loading between MEAs could result in slightly different cell performance. In addition, different flow field designs could also change contact resistances. These problems can be solved by tuning some parameters in the cell voltage model. Overall, we judge the model prediction accuracy to be quite satisfactory. We think this segmented model can be reconnected to predict the performance of cells with different flow field design, and this is useful as a tool to assess cell designs before those cells are actually machined, assembled and tested.

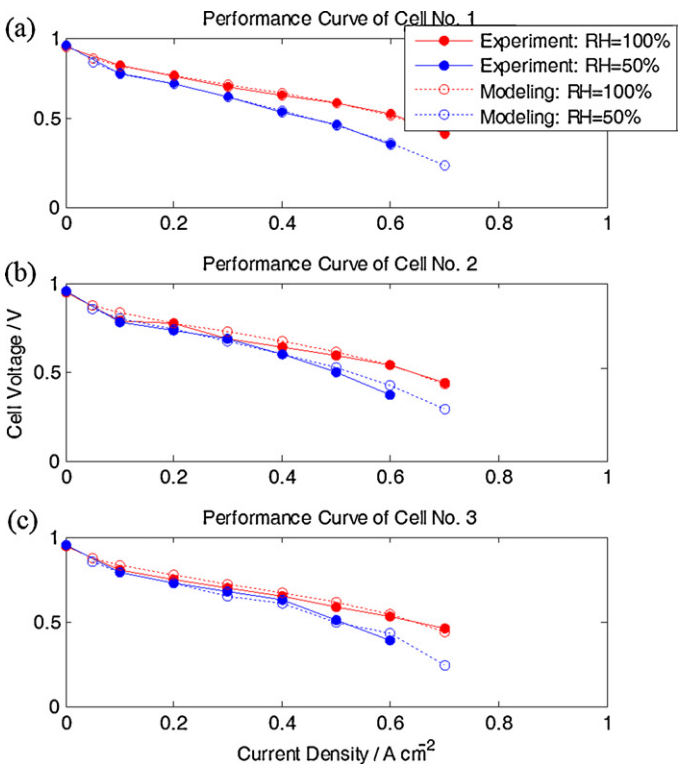

Fig. 8. Comparison of experimental results and modeling results for different cathode inlet RH values. (a) Cell No. 1; (b) cell No. 2; (c) cell No. 3.

Fig. 9 shows current density distribution, water content in the membrane, and RH values in the anode and cathode channels of cell No. 2 when the cathode inlet RH is 100% and 50%, respectively. When cathode inlet RH is 100%, current density distribution is more even than the case when the cathode inlet RH is 50%. When cathode inlet RH is 50%, the current density near cathode inlet is lower and increases with cathode gas flow distance, as shown in Fig. 9(b). The results also indicate that the cathode inlet RH significantly influences current density distribution. The current density distribution of cell No. 3 shows similar trend as that of cell No. 2, i.e., the current density near the cathode inlet is the lowest and gradually increases toward the outlet, as shown in Fig. 10(b).

3.2. Comparison between modeling and experimental results

Figs. 11–13 compare the experimental data from RH sensors [19] and modeling results of RH distribution in the flow channels for cell No. 3. Fig. 11(c) shows that at high load, anode RH near the downstream area is lower than that at low current load, as shown in Fig. 11(b). A possible reason is the higher dry hydrogen flow rate at high current density, resulting in decreased RH in the down stream. The experimental data supports the modeling results, as shown in Fig. 11(c). In Fig. 12, when the cathode inlet RH is 50%, the modeling results also show good agreement with experimental data.

In Fig. 13(b), at low load the RH in the cathode channels also shows similar results as experimental data. However, at high current density condition, the model predicted RH in the downstream area is 100%, as shown in Fig. 13(c), but test results are around 60% as presented in Fig. 13(a). A possible reason is that we assumed that in our model liquid water is moved out of the cell at the same velocity as gas, so there is some liquid water in the downstream area of the cathode channels. However, because channel number is reduced from twelve to six, gas velocity in the downstream channels increases, resulting in the quick removal of liquid

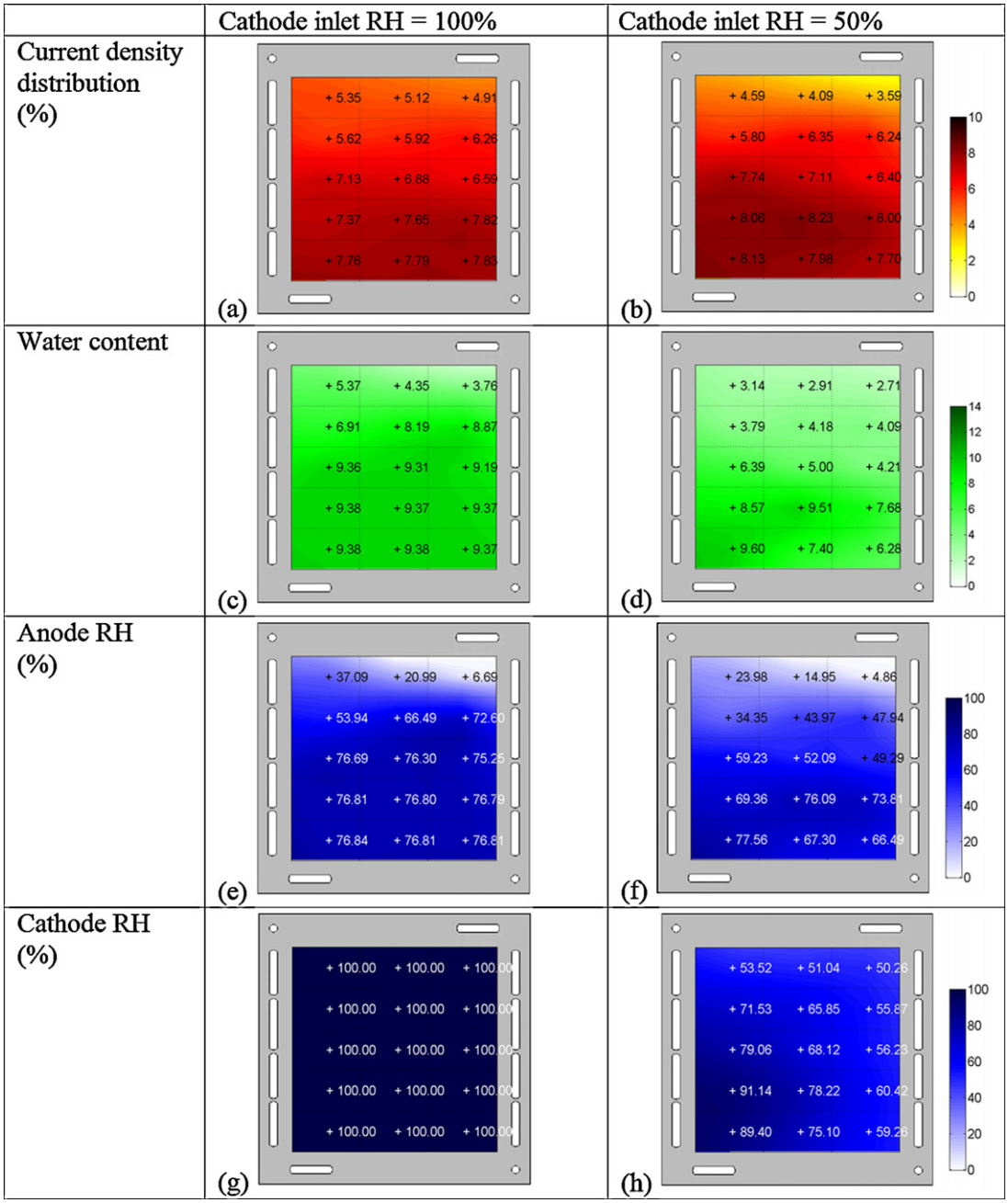

Fig. 9. Distributions of current density, water content in the membrane, RH in the anode channels, and RH in the cathode channels. Left figures: cathode inlet RH = 100%; right figures: cathode inlet RH = 50% (cell No. 2).

water. Besides, the under-saturated cathode gas also contributes to lower RH in the downstream channels.

Figs. 14 and 15 compare modeling results and experimental data of water distribution in cells No. 2 and 3, respectively. In Fig. 14, modeling results agree well with experimental data for most of the operating conditions except at low current loads. According to the results shown in Fig. 15, this model successfully predicts water accumulation in the majority of segments for most of the operating conditions. The variation between modeling results and experimental data could be due to a few different reasons. First, the model parameters were calibrated based on the experimental data of cell No. 1. The influence of flow field patterns on the parameters was not considered. Second, the experimental data of water accumulation was quantified "indirectly" by using the least-squares method, which was described in our previous study [19]. An improved experimental design to "directly" measure water accumulation in the GDL is needed for accuracy when water accumulation is considered in the model.

3.3. New flow field design

According to the above results, high RH value of cathode inlet gas helps the cell current to be distributed more evenly. Liu et al. [20] measured the current density distribution of a working fuel cell; they also observed this phenomenon in their study. This phenomenon can be explained by the membrane hydration model, in

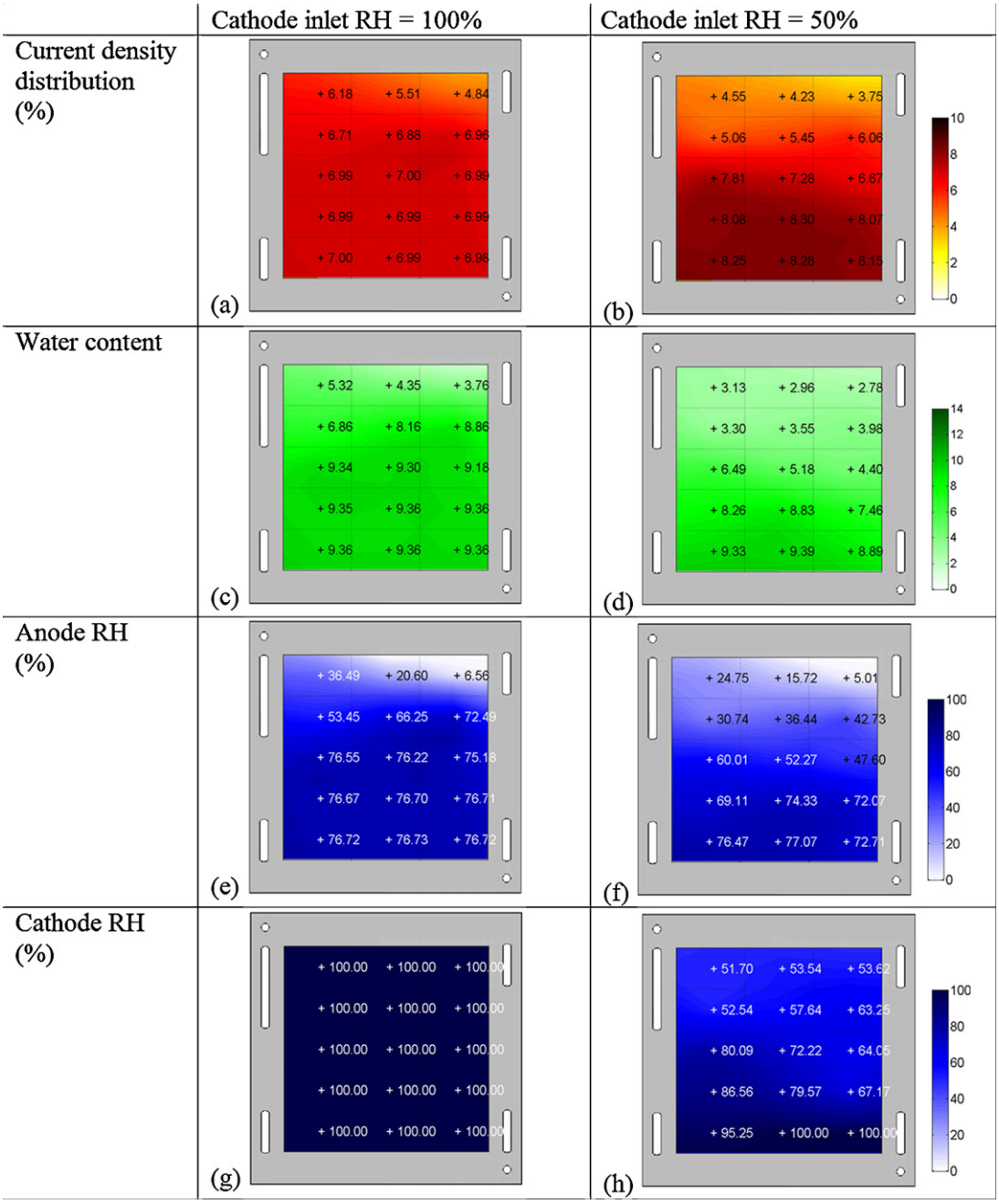

Fig. 10. Distributions of current density, water content in the membrane, RH in the anode channels, and RH in the cathode channels. Left figures: cathode inlet RH = 100%; right figures: cathode inlet RH = 50% (cell No. 3).

which water content in the membrane is determined by the RH values in the anode and cathode [21], as shown below:

$$\lambda_{pem}=0.043+17.81a_{pem}-39.85a_{pem}^2+36.0a_{pem}^3, \quad 0<a_{pem}\leq 1 \tag{10}$$

$$a_{pem}=\frac{a_{an}+a_{ca}}{2} \tag{11}$$

At the operating conditions where the cathode inlet RH is 50%, the RH values in the anode and cathode channels increase with flow direction. If the cathode flow direction is opposite to the anode flow direction, the overall water content in the membrane will be more even due to the fact reactants are more humid at the downstream. When a humidifier is not available, counter-flow field design is a good solution.

In portable fuel cell systems or transportation applications, where there is limited space for humidifiers, an appropriate flow field design may help to increase the system efficiency. Under the circumstances where humidifiers cannot work efficiently or are not available, generated liquid water within the fuel cell should be used effectively to hydrate the membrane internally. In the flow pattern design of cells No. 1, 2, and 3, both the anode and cathode reactants move from the top to the bottom. Thus, we designed a virtual cell No. 4, in which the cathode inlet is placed at the bottom of the active area and the anode flow direction is kept the same as the other cells, as shown in Fig. 16. The performance and water accumulation in this design is predicted by our segmented model and compared with other designs.

Fig. 17 shows the modeling results of cell No. 4. In the working condition where the cathode inlet RH is 100%, the distributions of

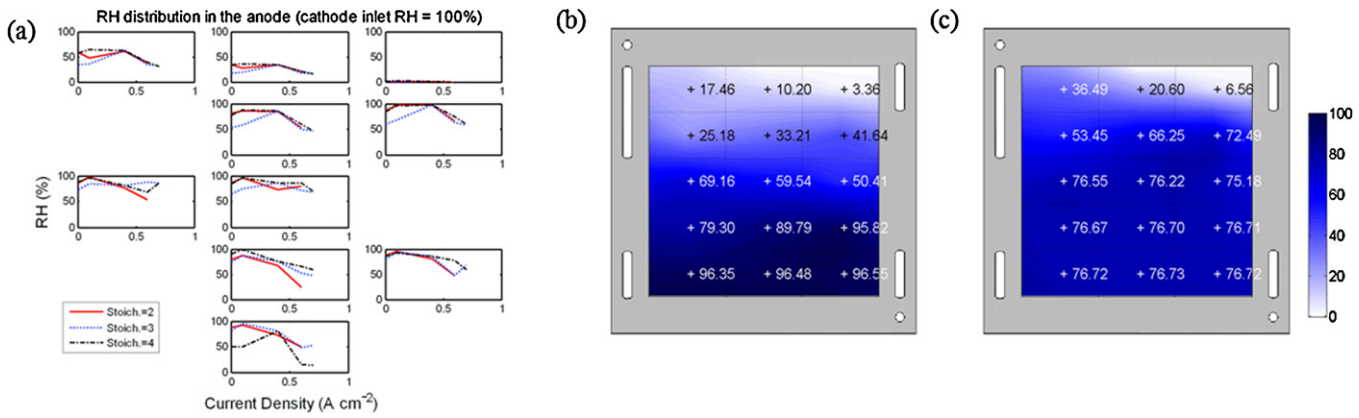

Fig. 11. RH in the anode flow channels when cathode inlet RH is 100% (cell No. 3) (a) experimental results; (b) modeling results when current density is 0.1 A cm^{-2}; (c) modeling results when current density is 0.7 A cm^{-2}.

current density and water content in the membrane are similar to those of cells No. 1, 2, and 3 at the same operating condition. However, when the cathode inlet RH is 50%, the current density near the anode inlet of cell No. 4 (4.72%) is higher than those of cells No. 1 (3.90%) [14], No. 2 (3.59%), and No. 3 (3.75%). The current densities at the bottom segments of cell No. 4 are lower because under-saturated cathode reactant is fed from the bottom of the cell. The maximum current density appears in the middle part of the active area, as shown in Fig. 17(b), and the distribution is more uniform through the whole active area when compared with that of cells No, 1, 2, and 3. Water content in the membrane shows similar trend as current density distribution, as shown in Fig. 17(d). The performance of these four flow pattern designs was compared in Fig. 18. There is no significant difference when the cathode inlet RH is 100%. When the RH of cathode inlet is 50%, however, cell No. 4 shows higher performance than the other cells do, especially at high load. This is mainly due to the humid cathode reactant near the outlet, resulting in increased water content in the membrane.

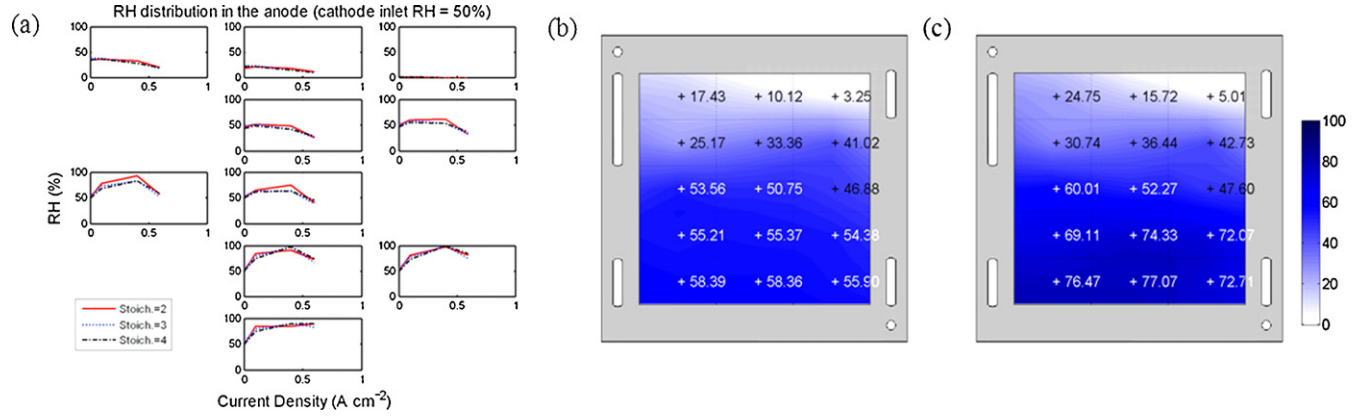

Fig. 12. RH in the anode flow channels when cathode inlet RH is 50% (cell No. 3) (a) experimental results; (b) modeling results when current density is 0.1 A cm^{-2}; (c) modeling results when current density is 0.6 A cm^{-2}.

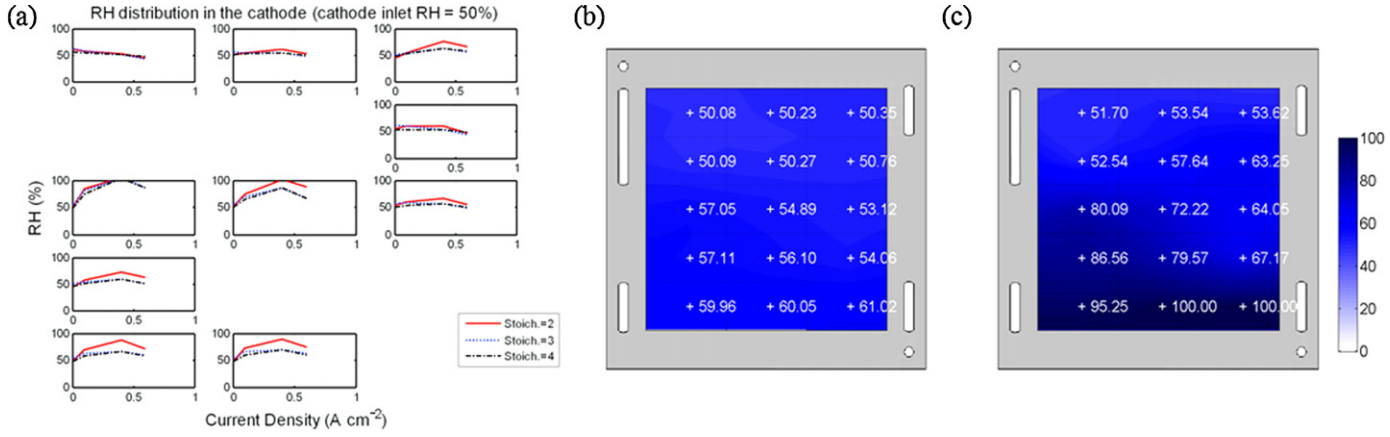

Fig. 13. RH in the cathode flow channels when cathode inlet RH is 50% (cell No. 3) (a) experimental results; (b) modeling results when current density is 0.1 A cm^{-2}; (c) modeling results when current density is 0.6 A cm^{-2}.

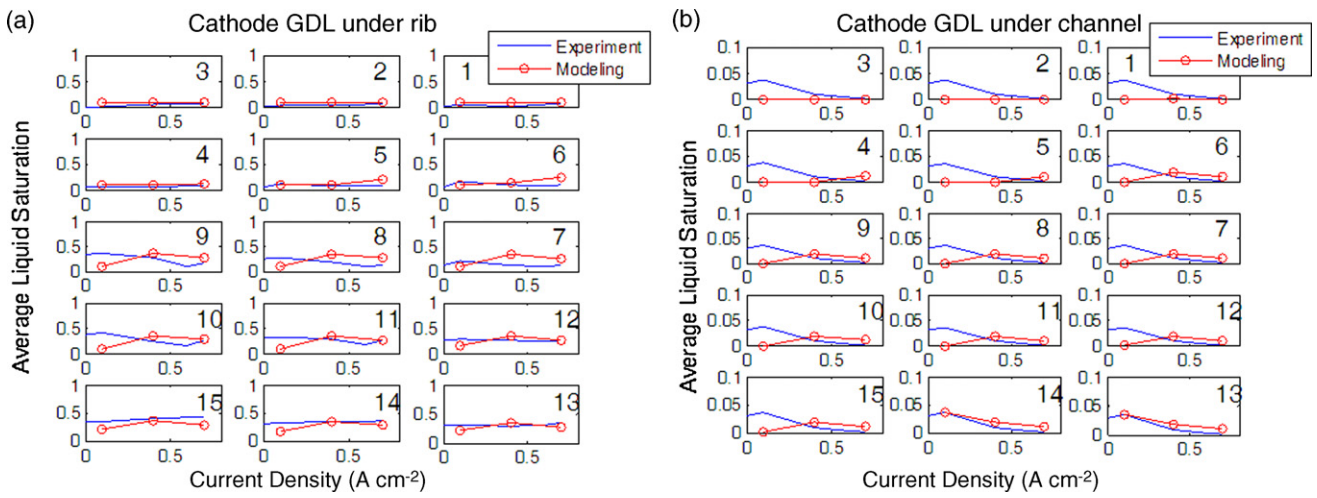

Fig. 14. Comparison of average liquid saturations from modeling results and experimental data (cell No. 2) (a) distribution of average liquid saturation in the cathode GDL under rib; (b) distribution of average liquid saturation in the cathode GDL under channel.

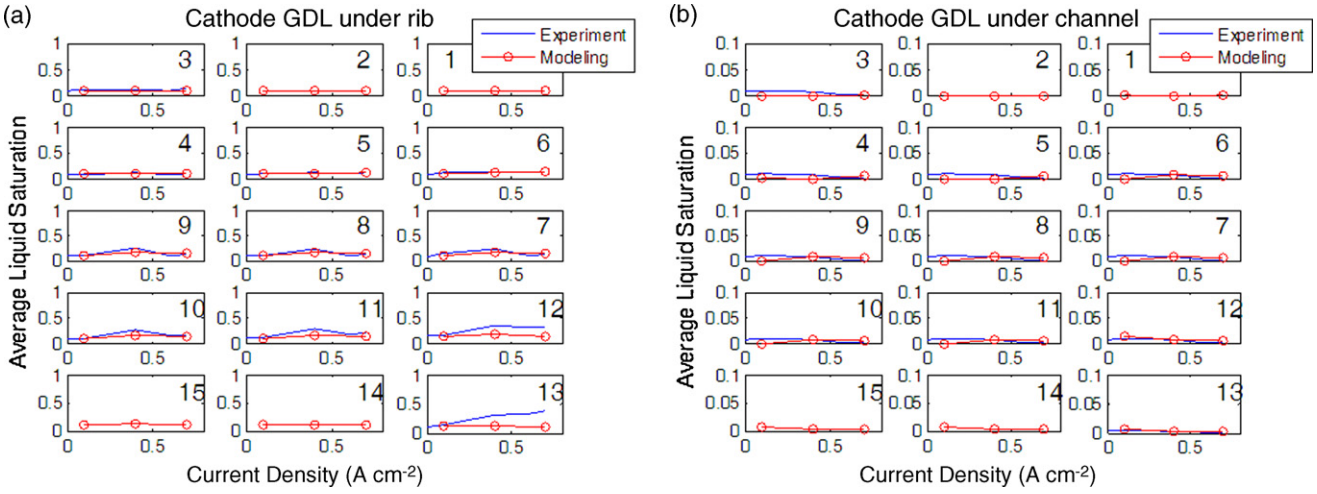

Fig. 15. Comparison of average liquid saturations from modeling results and experimental data (cell No. 3) (a) distribution of average liquid saturation in the cathode GDL under rib; (b) distribution of average liquid saturation in the cathode GDL under channel.

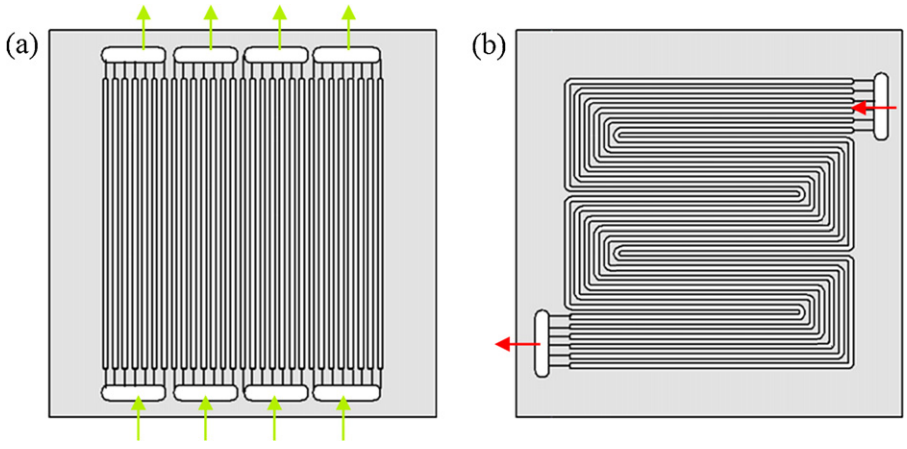

Fig. 16. Flow field pattern of cell No. 4. (a) The cathode inlet is placed at the bottom of the active area. (b) The anode inlet is on the upper right corner.

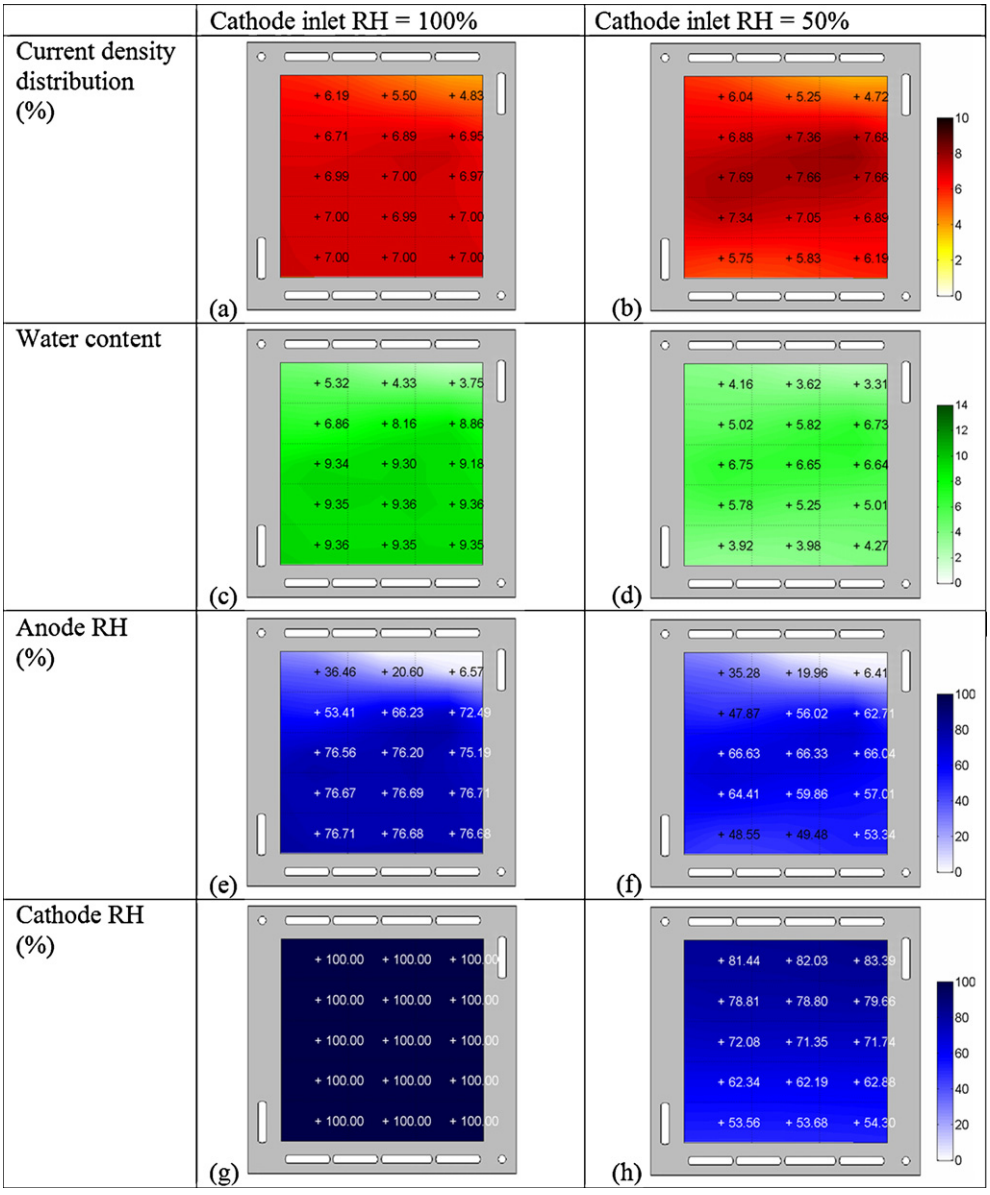

Fig. 17. Distributions of current density, water content in the membrane, RH in the anode channels, and RH in the cathode channels. Left figures: cathode inlet RH = 100%; right figures: cathode inlet RH = 50% (cell No. 4).

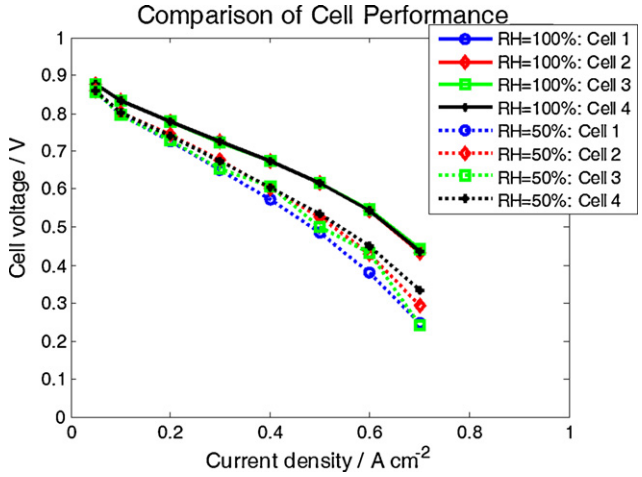

Fig. 18. Comparison of performances of four single cells.

4. Conclusions

In this work current density distributions within four single cells with different flow field patterns are predicted by using a segmented mathematical model. Each segment is viewed as a lumped element, which consists of six interacting sub-models, and is connected based on the reactant flow directions of individual fuel cells. This model is calibrated based on experimental data of one single cell and the segments in this model are reconnected according to flow field patterns of the other cells. The distributed properties, including water content in the membrane and relative humidity in the flow channels, are also investigated by this model. Modeling results show good agreement with experimental data under most working conditions.

We provide the segmented model and a feasible method to solve the problem in which co-flow and counter-flow exist in the flow field design. In the low humidity working conditions, current density of the first segment, which is near the inlet, takes approximately 3.9% of the current load in traditional flow field designs. The value

can be improved to 4.7% by placing the cathode flow direction opposite to the anode. The counter-flow design also makes water content in the membrane distributed more uniformly; thus, the durability and efficiency of the fuel cell can be improved.

References

[1] W.-M. Yan, C.-Y. Chen, S.-C. Mei, C.-Y. Soong, F. Chen, J. Power sources 162 (2006) 1157–1164.
[2] X. Zhang, T. Wang, D. Zheng, J. Zhang, Y. Zhang, L. Zhu, C. Chen, J. Yan, H. Liu, Y. Lou, X. Li, B. Xia, J. Electrochem. Sci. 2 (2007) 618–626.
[3] N.G. Vitale, US Patent 5,981,098 (1999).
[4] J.K. Neutzler, US Patent 5,776,624 (1998).
[5] S. Um, C.Y. Wang, K.S. Chen, J. Power sources 125 (2004) 40–51.
[6] Z.H. Wang, C.Y. Wang, K.S. Wang, J. Power Sources 94 (2001) 40–50.
[7] U. Pasaogullari, C.Y. Wang, J. Electrochem. Soc. 151 (2004) A399–A406.
[8] A.S. Aricò, P. Cretì, V. Baglio, E. Modica, V. Antonucci, J. Power Sources 91 (2000) 202–209.
[9] H. Dohle, T. Bewer, J. Mergel, R. Hetzel, D. Stolten, Proceedings of Fuel Cell Seminar, Portland, OR, 2000, pp. 130–133.
[10] T. Bewer, T. Beckmann, H. Dohle, J. Mergel, D. Stolten, Proceedings of the First European PEFC forum (EFCF), 2001, pp. 321–330.
[11] T. Bewer, T. Beckmann, H. Dohle, J. Mergel, D. Stolten, J. Power Sources 125 (2004) 1–9.
[12] A. Kumar, R.G. Reddy, J. Power Sources 155 (2006) 264–271.
[13] J. Golbert, D.R. Lewin, J. Power Sources 135 (2004) 135–151.
[14] Y.-S. Chen, H. Peng, J. Power Sources 185 (2008) 1179–1192.
[15] S.-H. Ge, B.-L. Yi, J. Power Sources 124 (2003) 1–11.
[16] E. Birgersson, M. Vynnycky, J. Power Sources 153 (2006) 76–88.
[17] J.J. Hwang, C.H. Chaob, W.Y. Hoa, C.L. Changa, D.Y. Wang, J. Power Sources 157 (2006) 85–97.
[18] P. Berger, K. Promislow, St.J. Pierre, J. Stumper, B. Wetton, J. Electrochem. Soc. 151 (2004) A341–A353.
[19] Y.-S. Chen, H. Peng, J. Fuel Cell Sci. Technol. 6 (2009), 031016-1-031016-13.
[20] Z. Liu, Z. Mao, B. Wu, L. Wang, V.M. Schmidt, J. Power Sources 141 (2005) 205–210.
[21] T.E. Springer, T.A. Zawodzinski, S. Gottesfeld, J. Electrochem. Soc. 138 (1991) 2334–2342.